

PREDICTIONS OF LDEF RADIOACTIVITY AND
COMPARISON WITH MEASUREMENTS

T. W. Armstrong and B. L. Colborn
Science Applications International Corporation¹
Route 2, Prospect, TN 38477
Phone: 615/468-2603, Fax: 615/468-2676

B. A. Harmon
NASA Marshall Space Flight Center
Huntsville, AL 35812
Phone: 205/544-4924, Fax: 205/544-7754

C. E. Laird
Department of Physics, Eastern Kentucky University¹
Richmond, KY 40475
Phone: 606/622-1526, Fax: 606/622-1020

ABSTRACT

As part of the program to utilize LDEF data for evaluation and improvement of current ionizing radiation environment models and related predictive methods for future LEO missions, calculations have been carried out to compare with the induced radioactivity measured in metal samples placed on LDEF. The predicted activation is about a factor of two lower than observed, which is attributed to deficiencies in the AP8 trapped proton model. It is shown that this finding based on activation sample data is consistent with comparisons made with other LDEF activation and dose data. Plans for confirming these results utilizing additional LDEF data sets, and plans for model modifications to improve the agreement with LDEF data, are discussed.

INTRODUCTION

The measured activation of materials on LDEF from radioactivity induced by trapped proton and cosmic ray environments provides an important data set for checking the accuracy of environment models and associated calculational methods for predicting the activation of spacecraft and payload materials in low-Earth orbit. Such modeling accuracy is of particular interest in radiation background assessments and component material selection in the design of space-based sensors.

In the present work, predictions have been made to compare with the observed radioactivity in several metal samples intentionally placed on LDEF as activation experiments. Model comparisons with LDEF activation measurements of spacecraft components and with thermoluminescent dosimetry (TLD) data have been reported previously (refs. 1,2). A result from these previous model/data comparisons is an estimate of the accuracy of the current AP8 trapped proton model for low-Earth orbit applications. The activation experiment sample data considered here provide an important additional data set for model comparisons by allowing a consistency check of the different data sets, previous model/data comparisons, and previous conclusions related to quantifying the trapped proton environment modeling uncertainties.

¹Work supported by NASA Marshall Space Flight Center, Huntsville, Alabama.

The activation experiment samples consisted of the metals nickel, tantalum, vanadium, indium, and cobalt placed in experiment trays at various locations on LDEF (Table 1), with sample sizes typically 2 in. x 2 in. and either 0.125 or 0.25 in. thick (ref. 3). A total of some 20 radioisotopes have been measured from these samples. We have not made predictions to compare with all of the measured radioisotopes for the following reasons: First, the primary objective of the present calculations is to compare with those radioisotopes which are produced by primary trapped protons so that previous conclusions on the accuracy of the AP8 model derived from model comparisons with other LDEF data can be checked. Some estimates are included here for isotopes produced by secondary neutrons and galactic cosmic rays, but the calculational method used for these estimates is less rigorous than that used for the trapped proton produced isotopes. Secondly, the activation cross sections needed in predicting certain isotopes are not adequately known to provide the prediction accuracy needed in evaluating trapped proton model uncertainties. For these reasons, the predicted isotopes here are restricted to the nickel and vanadium samples.

The model comparisons made here with activation sample data provide a measure of the trapped proton flux model uncertainties, but information on the trapped proton anisotropy is difficult to interpret from these data because the samples are under different amounts of shielding at different locations (Table 2). The tray clamp activation data, which provide a detailed spatial mapping and are mostly free of shielding effects, provide a better data set for anisotropy model evaluations, as addressed in ref. 2.

The activation modeling approach has been to perform detailed calculations so that differences between the predicted and measured activations can be attributed to uncertainties in the incident radiation environment. Thus, as described below, predictions are based on a detailed treatment of the trapped proton environment (taking into account proton anisotropy, flux altitude dependence with mission time, and solar cycle dependence) and radiation transport using a detailed 3-D mass model of the LDEF spacecraft and experiment trays to account for shielding effects.

PREDICTION METHODS

Radiation Environment -- The LDEF trapped proton exposure predicted by Watts, et al. (ref. 4) is used, which is based on the AP8 omnidirectional flux model (ref. 5), the anisotropy model of Watts, et al. (ref. 6) to obtain directionality of the incident flux spectrum, a detailed altitude dependence during the LDEF mission, and an interpolation of the solar minimum (AP8MIN) and solar maximum (AP8MAX) versions of the AP8 model according to the F10.7 cm. solar flux to account for solar cycle variations of the proton flux during the mission. For incident galactic protons, the LDEF orbit-average exposure from ref. 7 was used, which is based on the interplanetary spectrum of Adams (ref. 8).

Shielding Model -- The 3-D mass model developed for LDEF radiation analyses (ref. 9) was used. This model was extended for the present calculations to incorporate each of the activation samples -- i.e., the actual size and location of all of the individual activation samples were included in the shielding model.

Radiation Transport -- For incident trapped protons, radiation transport calculations were made using the Burrell primary proton transport code (ref. 10) and the 3-D mass model of LDEF with the activation samples included. At each spatial point in the activation samples where flux spectra were calculated, an angular grid of 720 equal solid angle bins around the point was defined, with a different energy spectrum incident in each solid angle to account for the trapped proton directionality. For examining activation produced by incident galactic protons, particle spectra (primary protons, secondary neutrons and protons) from previous (ref. 7) Monte Carlo (HETC code) transport calculations for a simple geometry model (1-D slab of aluminum) were used. Thus, the activation estimates from the galactic environment is approximate due to the geometry simplification, but, as discussed above, the trapped proton activation is the main interest here.

Radioisotope Production -- Flux spectra calculated at the center of each activation sample were folded with measured activation cross sections (shown later) compiled from the literature to compute radioisotope production as a function of time during the mission, with decay rates then applied to obtain the radioactivity at LDEF recovery. (As a check on the approximation of using the flux only at the center of the sample, volume-average fluxes from a fine grid of flux points were computed for several samples and compared with the single point flux; the resulting activations agreed to within about 10% or less).

PREDICTED VS. MEASURED SAMPLE ACTIVATION

A summary of the LDEF activation sample measurement results is given in Table 3. Final data analyses and intercomparisons of measurements at different facilities have not yet been completed for all of the isotopes produced (ref. 11), so the data shown here are preliminary at present.

Vanadium Activation

Activation data for the vanadium sample are well suited for model comparisons because vanadium has a single target isotope (99.75% ^{51}V) and a single measured radioisotope (^{46}Sc), so the production mode is well defined for predictions; the activation cross section is well known (Fig. 1); and the energy threshold for ^{46}Sc production is relatively low (≈ 30 MeV), so the production is almost all ($\approx 96\%$) from incident primary trapped protons rather than from secondaries or galactic cosmic rays.

A comparison of the measured and calculated ^{46}Sc activation for the vanadium samples is shown in Fig. 2. Both the measured and calculated activities indicate only a small dependence on sample locations, suggesting that differences that might be expected due to the trapped proton anisotropy are masked by differences in shielding (Table 2). The average ratio of predicted to measured activity for samples at all locations is 0.49 ± 0.11 .

Nickel Activation

Predictions for the nickel sample activation are not as simple as for vanadium because there are various production modes (Table 4), requiring a large number of activation cross sections (e.g., Fig. 3 for proton induced reactions), and secondary neutrons are important in producing some of the isotopes. A comparison of predicted vs. measured activities for the nickel sample in Exp. P0006 (Fig. 4) shows that trapped protons dominate the production of ^{54}Mn and ^{56}Co , but neutrons dominate the ^{58}Co and ^{60}Co production, and cosmic rays dominate the ^{46}Sc production due to its high energy threshold. The calculated and measured activities for nickel samples at all locations are compared in Table 5. The average ratio of predicted-to-measured activities for the two isotopes (^{54}Mn and ^{56}Co) produced by primary trapped protons for all samples is $0.56 \pm \approx 0.08$.

Solar Minimum vs. Solar Maximum Activation

Since LDEF exposure to trapped protons during the early part of the mission was at solar minimum and during the latter part at solar maximum (Fig. 5), activities for long vs. short half-life isotopes can be used to investigate uncertainty differences in the solar minimum (AP8MIN) vs. solar maximum (AP8MAX) trapped proton models. For example, Fig. 6 shows the case of a relatively short half-life product (^{46}Sc from V sample in Exp. P0006, 84 day half-life). Two curves are shown: the production rate vs. mission time, and the contribution of the production at times during the mission to the activity at recovery, which shows that the recovery activity for this isotope is due to proton exposure during solar maximum. The predicted-to-measured activity ratio in this case is 0.49 ± 0.11 . For a long half-life

isotope where the activity is at recovery due exposure during solar minimum, we use the ^{54}Mn activity (half-life = 303 days) for the same nickel sample in Exp. P0006, for which the predicted/measured ratio is 0.60 ± 0.12 . Therefore, from comparisons with LDEF activation data we find no major difference in the AP8MIN vs. AP8MAX model uncertainties.

MODEL COMPARISONS WITH OTHER LDEF RADIATION DATA

The above comparisons of predicted vs. measured activities for the activation samples placed on LDEF indicate that the AP8 model underpredicts the trapped proton flux for the LDEF mission by about a factor of two. This result is consistent with model comparisons with other LDEF data, as summarized below.

Figure 7 compares predicted and measured ^{22}Na production in the aluminum clamps holding the experiment trays on LDEF, which has been published previously (ref. 2). The average predicted/measured activation around the spacecraft is $0.55 \pm$ about 0.15 (Fig. 7). This ratio is in agreement with dose predictions that have been compared (ref.1) with TLD doses measured on LDEF (ref. 12) at shielding depths where the dose is due to trapped protons.

Figure 8 summarizes predicted vs. measured results for three different sets of data (tray clamp activity, TLD dose, and radioisotopes in activation samples) at the same location on LDEF (Exp. P0006 in Tray F2). These results show that the model/data comparisons are consistent for the different data sets and that the predictions are about a factor of two lower than all of the data sets.

Another data set suitable for including in the comparisons of Fig. 8 is the fission tracks measured from fission foils (^{181}Ta , ^{209}Bi , ^{232}Th , and ^{238}U) included in Exp. P0006 (ref. 13). While these foils respond to protons and neutrons from both trapped and galactic proton sources, an estimate based on particle spectra from 1-D Monte Carlo calculations (ref. 7) shows that the energy dependence of the fission cross section for the Bi foil is such that fission tracks are produced predominately by trapped protons. Detailed calculations taking into account 3-D shielding effects have not yet been made to compare with these data.

Preliminary comparisons of predicted vs. measured activation of the steel trunnions on LDEF, which indicate somewhat better agreement than determined here for the activation samples, have been reported (ref. 14). However, this early work was of a scoping nature and several approximations were made in the predictions (e.g., the current estimate, ref. 4, of the trapped proton environment for LDEF was not available at that time), so these early trunnion activation calculations need to be revised before definitive trunnion data comparisons can be obtained.

SUMMARY

The predictions made here for the activation of metal samples placed on LDEF confirm results from previous comparisons with spacecraft component (tray clamp) activation data and TLD dosimetry data that radiation effects measured on LDEF that are due to the trapped proton environment are underpredicted by about a factor of two. These results indicate that the AP8 trapped proton model underpredicts the actual environment by a factor of two. Additional calculations to compare with other data sets (trunnion activation and fission foil measurements) are planned to further check this conclusion.

An investigation of model improvements that would give better agreement with the LDEF data is also planned. For example, predicted vs. measured differences for the trapped proton anisotropy is likely due to the approximate nature of the effective atmospheric scale heights currently used as input to the

anisotropy model, and work to determine more accurate effective scale height estimates is planned. Also, recent work at the European Space Agency (ESA), ref. 15, shows that improvement to some of the numerical interpolation procedures used in the AP8 model increases the predicted trapped proton flux for low-Earth orbits, and comparisons with LDEF data using the ESA version of the AP8 model are planned.

REFERENCES

1. Armstrong, T. W. and Colborn, B. L.: Radiation Model Predictions and Validation Using LDEF Satellite Data. Second LDEF Post-Retrieval Symposium, NASA CP-3194, 1993.
2. Armstrong, T. W.; Colborn, B. L.; Harmon, B. A.; Parnell, T. A.; Watts, J. W. and Benton, E. V.: Comparison of Model Predictions with LDEF Satellite Radiation Measurements. *Adv. Space Res.* 14, No. 10, 17 (1994).
3. Harmon, B. A.; Fishman, G. F.; Parnell, T. A.; Benton, E. V. and Frank, A. L.: LDEF Radiation Measurements: Preliminary Results. *Nucl. Tracks Radiat. Meas.* 20, 131 (1992).
4. Watts, J. W.; Armstrong, T. W. and Colborn, B. L.: Revised Predictions of LDEF Exposure to Trapped Protons. Second LDEF Post-Retrieval Symposium, NASA CP-3194, 1993.
5. Sawyer, Donald W. and Vette, James I.: AP8 Trapped Proton Environment for Solar Maximum and Solar Minimum. National Science Data Center, Goddard Space Flight Center, NSSDC/WDC-A-R&S 76-06, Dec. 1976.
6. Watts, J. W., Jr.; Parnell, T. A. and Heckman, H. H.: Approximate Angular Distribution and Spectra for Geomagnetically Trapped Protons in Low-Earth Orbit, in: *High Energy Radiation Background in Space*, Proc. AIP Conf., Vol. 186, pp. 75-85, American Institute of Physics, New York, 1989.
7. Armstrong, T. W. and Colborn, B. L.: Predictions of Induced Radioactivity for Spacecraft in Low-Earth Orbit. *Nucl. Tracks Radiat. Meas.* 20, 101 (1992).
8. Adams, James H., Jr.: Cosmic Ray Effects on Microelectronics. Part IV. NRL Memorandum Report 5901, December 1986.
9. Colborn, B. L. and Armstrong, T. W.: Development and Application of a 3-D Geometry/Mass Model for LDEF Satellite Ionizing Radiation Assessments. Second LDEF Post-Retrieval Symposium, NASA CP-3194, 1993.
10. Burrell, M. O.: The Calculation of Proton Penetration and Dose Rates. George C. Marshall Space Flight Center, Huntsville, AL., NASA TM X-53063, August 1964.
11. Harmon, Alan B.; Parnell, Thomas A. and Laird, Christopher E.: Status of LDEF Activation Measurements and Archive. (These Proceedings).
12. Frank, A. L.; Benton, E. V.; Armstrong, T. W. and Colborn, B. L.: Absorbed Dose Measurements and Predictions on LDEF. Second LDEF Post-Retrieval Symposium, NASA CP-3194, 1993.
13. Benton, E. V.: LDEF Experiment P0006 Linear Energy Transfer Spectra Measurement (LETSME). Evil Research, Inc. Final Report to NASA Marshall Space Flight Center, December 1990.

REFERENCES (CONT'D)

14. Armstrong, T. W.; Colborn, B. L. and Watts, J. W.: Ionizing Radiation Calculations and Comparisons with LDEF Data. First LDEF Post-Retrieval Symposium, NASA CP-3134, 1991.
15. Daly, E. J. and Evans, H. D. R.: Problems in Radiation Environment Models at Low Altitudes. European Space Agency/ESTEC, preprint.
16. Smith, Alan R. and Hurley, Donna L.: Radioactivities of Long Duration Exposure Facility (LDEF) Materials: Baggage and Bonanzas. First LDEF Post-Retrieval Symposium, NASA CP-3134, 1991.
17. Winn, Willard G.: Gamma-ray Spectrometry of LDEF Samples at SRL. First LDEF Post-Retrieval Symposium, NASA CP-3134, 1991.
18. Laird, Christopher E.: Eastern Kentucky Univ., pri. comm.
19. Harmon, B. A.; Fishman, G. J.; Parnell, T. A. and Laird, C. E.: Induced Activation Study of LDEF. Second LDEF Post-Retrieval Symposium, NASA CP-3194, 1993.
20. Reeves, James H.; Arthur, Richard J. and Brodzinski, Ronald L.: Sensitivity of LDEF Foil Analyses Using Ultra-Low Background Germanium vs. Large NaI (TI) Multidimensional Spectrometers. Second LDEF Post Retrieval Symposium, NASA CP-3194.
21. Harmon, B. Alan: NASA Marshall Space Flight Center, pri. comm.

Table 1. Location of activation samples on LDEF.

Contained in Exp. No.	Exp. Tray	Tray Position	Activation Samples				
			Co	Ni	V	Ta	In
P0006	F2	Trailing Side		Ni	V	Ta	In
A0114	C9	Leading Side	Co			Ta	In
A0114	C3	Trailing Side		Ni	V		
M0001	H12	Space End	Co	Ni	V	Ta	In
M0002	G12	Earth End	Co	Ni	V	Ta	In

Table 2. Vertical shielding for activation samples.

Sample	Vertical shielding (g/cm^2) of activation sample in LDEF experiment tray:				
	H-12	G-12	C-3	C-9	F-2
V	thermal cover	2.8	1.7		13
Ni	thermal cover	2.8	1.7		13
Co	thermal cover			1.7	13
Ta	thermal cover	8.0		1.7	13
In	thermal cover	8.0		1.7	13

Table 3. Summary of LDEF activation sample measurements - preliminary.

Activation Sample	Product Isotope	Tray H12 (space end) Exp. M0001		Tray G12 (Earth end) Exp. M0002		Tray C9 (leading side) Exp. A0114		Tray C3 (trailing side) Exp. A0114		Tray F2 (trailing side) Exp. P0006	
		Activity (pCi/kg)	Ref.	Activity (pCi/kg)	Ref.	Activity (pCi/kg)	Ref.	Activity (pCi/kg)	Ref.	Activity (pCi/kg)	Ref.
Nickel	Sc-46							11 ± 4 (c)		1.6 ± 0.4 (a)	
	Mn-54	52 ± 7.8 (c)		25 ± 3.4 (e)				68 ± 6 (c)		27 ± 0.9 (a)	
		72 ± 3.6 (d)		39 ± 8 (c)							
	Co-56	66 ± 28 (c)		29 ± 4.8 (e)				61 ± 9 (c)		33 ± 1.3 (a)	
		70 ± 2.6 (d)		62 ± 27 (c)						67 ± 16 (c)	
	Co-57	400 ± 7.2 (c)		403 ± 35 (e)				466 ± 18 (c)		322 ± 2 (a)	
395 ± 15 (d)			399 ± 23 (c)						360 ± 24 (c)		
Co-58	73 ± 3.4 (d)		62 ± 7.3 (e)				59 ± 11 (c)		42 ± 1.6 (a)		
			93 ± 17 (c)						69 ± 11 (c)		
Co-60	7.6 ± 3.4 (d)						11 ± 4 (c)		4.7 ± 0.3 (a)		
	9.0 ± 0.87 (g)										
	12 ± 7.8 (c)										
Tantalum	Lu-172	56 ± 2.1 (h)		40 ± 1 (h)				75 ± 2 (h)		47 ± 1 (h)	
	Lu-173	120 ± 9.8 (h)		171 ± 12 (h)				143 ± 5 (h)		91 ± 4 (h)	
										161 ± 8.3 (a)	
	Hf-175	38 ± 5.7 (h)		19 ± 2 (h)				39 ± 2 (h)		25 ± 2 (h)	
Ta-182									37 ± 1.9 (a)		
	116 ± 8.1 (h)		45 ± 4 (h)				38 ± 2 (h)		135 ± 4 (h)		
Vanadium	Sc-46	21 ± 6.0 (b)		16 ± 1.3 (b)		20 ± 1.5 (b)				17 ± 1.1 (a)	
		13 ± 1.7 (g)		16 ± 1.4 (e)		24 ± 2.0 (h)				21 ± 2.7 (c)	
Indium	Rh-102										
		2.2 ± 0.6 (a)		2.3 ± 0.3 (a)		3.2 ± 0.4 (a)				2.2 ± 0.9 (a)	
	Ag-110m	3.2 ± 0.8 (a)		2.3 ± 0.3 (a)		3.9 ± 0.5 (a)				5.1 ± 1.0 (a)	
	Sn-113	35 ± 4.2 (a)		21 ± 1.2 (a)		41 ± 2.7 (a)				54 ± 3.6 (a)	
			22 ± 3.8 (e)		47 ± 19 (c)						
In-114m	190 ± 115 (a)		35 ± 15 (a)		55 ± 35 (a)				105 ± 20 (a)		
Cobalt	Mn-54			91 ± 3.8 (e)		41 ± 1.1 (a)					
				62 ± 1.4 (f)							
	Co-56			22 ± 3.8 (e)							
	Co-57			303 ± 5.4 (e)		125 ± 1.6 (a)					
				211 ± 1.6 (f)							
Co-58			116 ± 20 (e)								
Co-60	204 ± 20 (g)		26 ± 2.2 (e)		19 ± 0.5 (a)						
			23 ± 0.8 (f)		27 ± 2.7 (g)						

- (a) LBL measurements (Smith and Hurley, ref. 16)
- (b) SRL measurements (Winn, ref. 17)
- (c) MSFC/EKU measurements (Laird, ref. 18))
- (d) Battelle measurements (from Laird, ref. 18)

- (e) LLNL measurements (Camp, from Harmon, ref. 19)
- (f) LBL measurements (Smith and Hurley, from Harmon, ref. 19)
- (g) Battelle measurements (Reaves, ref. 20)
- (h) JSC measurements (D. Lindstrom, ref. 21)

Table 4. Production modes for nickel activation products.

Product	Half-life	Production by Protons	Production by Neutrons	Production by Decay
Sc-46	83.8 days	Ni-58 (p,8p5n) Sc-46 Ni-60 (p,8p7n) Sc-46		
Mn-54	303 days	Ni-58 (p,4p1n) Mn-54 Ni-60 (p,4p3n) Mn-54		
Co-56	77 days	Ni-58 (p,2p1n) Co-56 Ni-60 (p,2p3n) Co-56		Ni-58(p,p2n)Ni-56 $\xrightarrow[6.1\text{ d}]{\text{EC}}$ Co-56
Co-57	270 days	Ni-58 (p,2p) Co-57 Ni-60 (p,2p2n) Co-57	Ni-58 (n,np) Co-57	Ni-58(p,pn)Ni-57 $\xrightarrow[36\text{ hr}]{\text{EC},\beta^+}$ Co-57
Co-58	71.3 days	Ni-60 (p,2pn) Co-58	Ni-58 (n,p) Co-58	Co-58m $\xrightarrow{9.2\text{ hr}}$ Co-58g
Co-60	5.26 years	Ni-62 (p,2pn) Co-60	Ni-60 (n,p) Co-60	Co-60m $\xrightarrow{10.5\text{m}}$ Co-60g

Table 5. Ratio of predicted-to-measured activity at recovery for nickel activation samples.

Isotope	Sample Location on LDEF			
	Exp. P0006	Exp. A0114	Exp. M0002	Exp. M0001
Sc-46	0.29			
Mn-54	0.62	0.34	0.58	0.38
Co-56	0.44	0.69	0.78	0.64
Co-57	0.46	0.48	0.46	0.63
Co-58	0.53	0.70	0.44	0.57
Co-60	0.84	0.50		
AVERAGE:	0.53	0.54	0.57	0.55
Average for all isotopes in all samples: 0.55 ± 0.1				

Data Sources: Harmon (NASA MSFC)
Laird (EKU)

Smith and Hurley (LBL)
Camp (LLNL)

Reeves (PNWL)

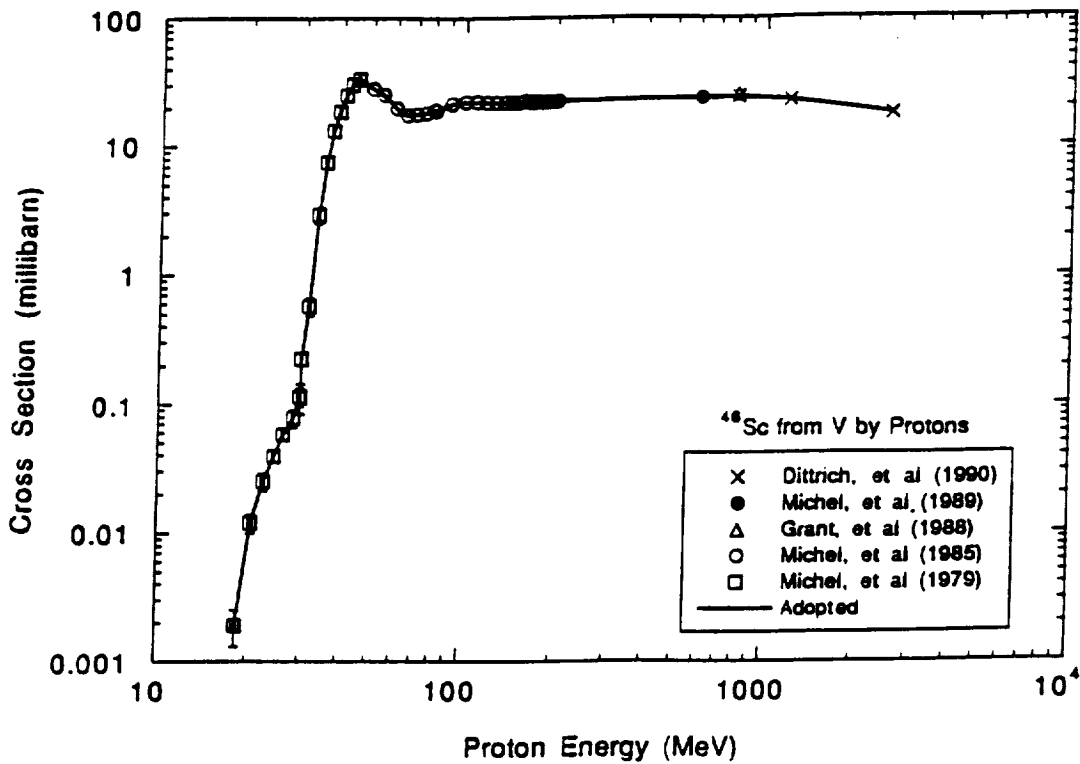


Fig. 1. Cross section for the production of ⁴⁶Sc from vanadium by protons; points represent measured cross sections.

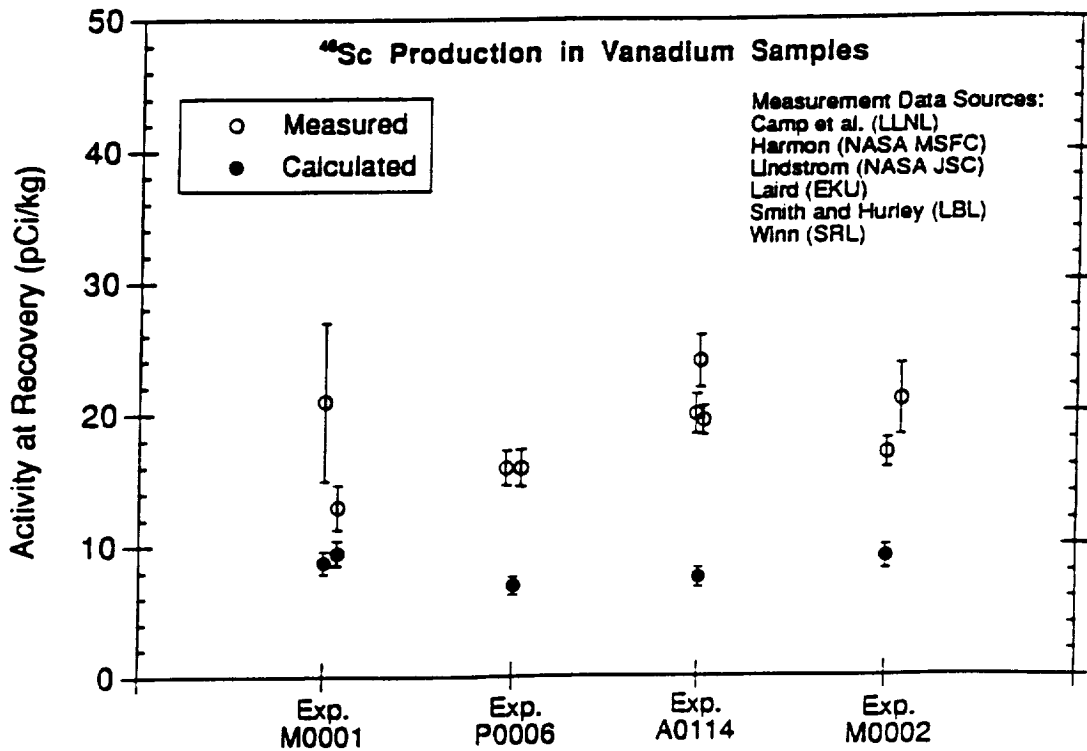


Fig. 2. Comparison of calculated and measured ⁴⁶Sc activation from vanadium samples.

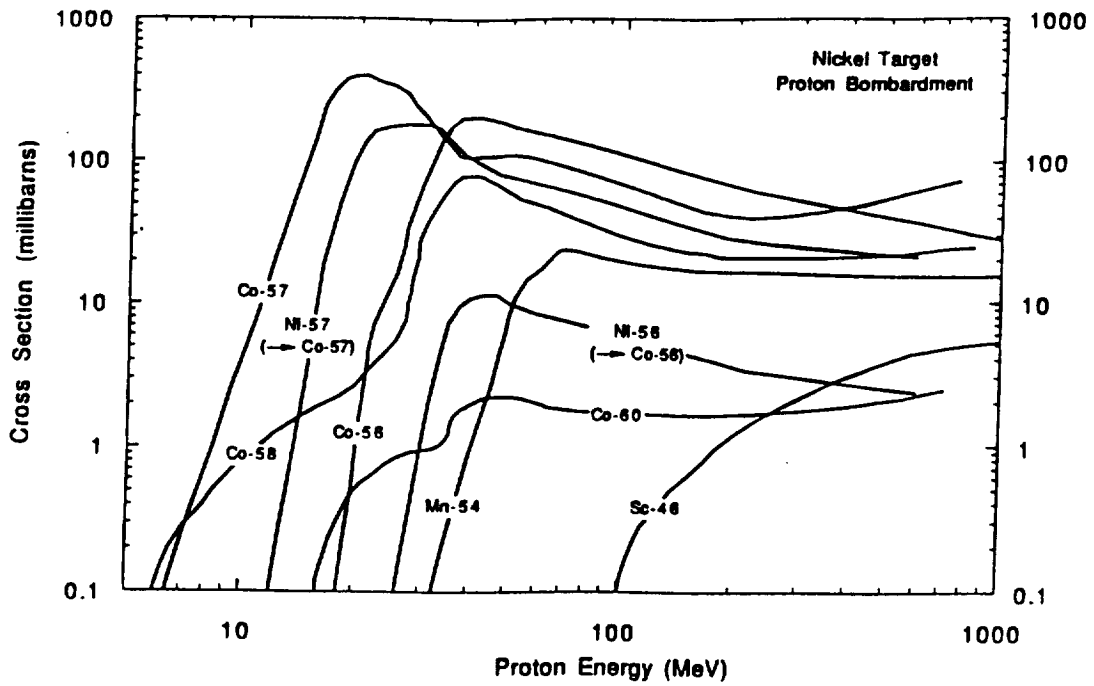


Fig. 3. Cross sections for the production of radioisotopes in nickel by protons, based on measured cross sections compiled from various sources.

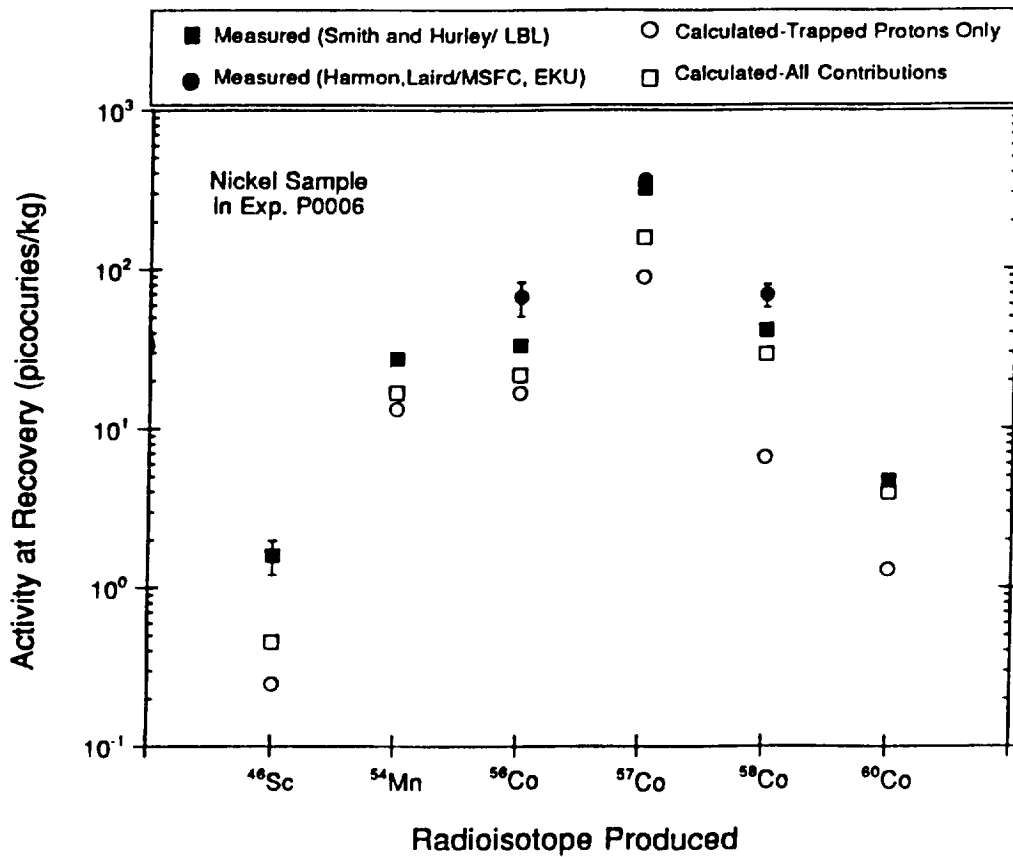


Figure 4. Comparison of predicted vs. measured (preliminary) activation products from nickel sample contained in LDEF Exp. P0006.

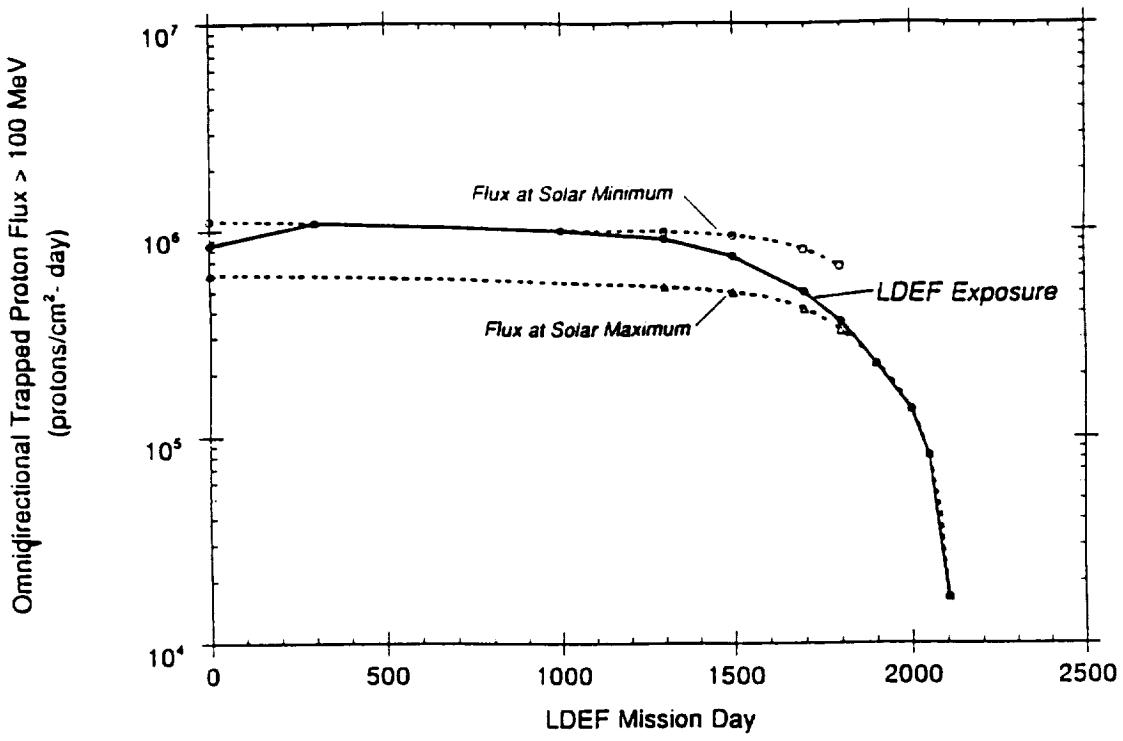


Fig. 5. Predicted trapped proton flux > 100 MeV during LDEF mission, from ref. 4.

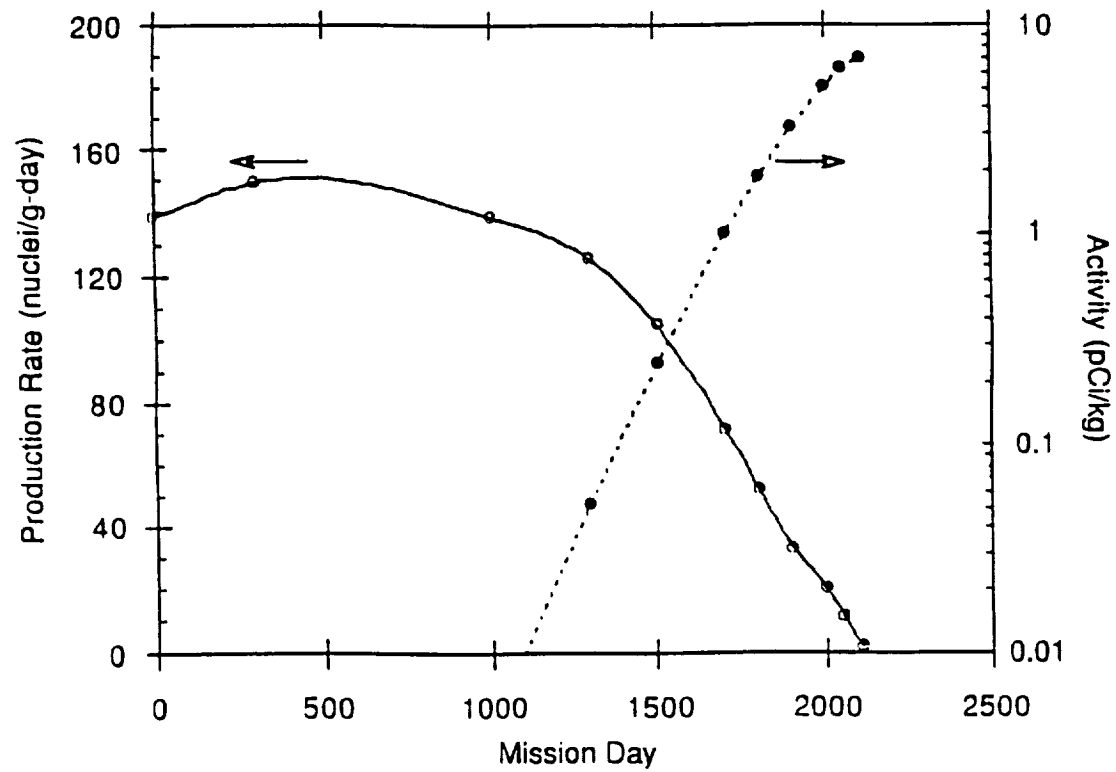


Fig. 6. Time dependence of ⁴⁶Sc production (solid curve) and the contribution of this production to the activity at recovery (dotted curve) for vanadium sample in Exp. P0006.

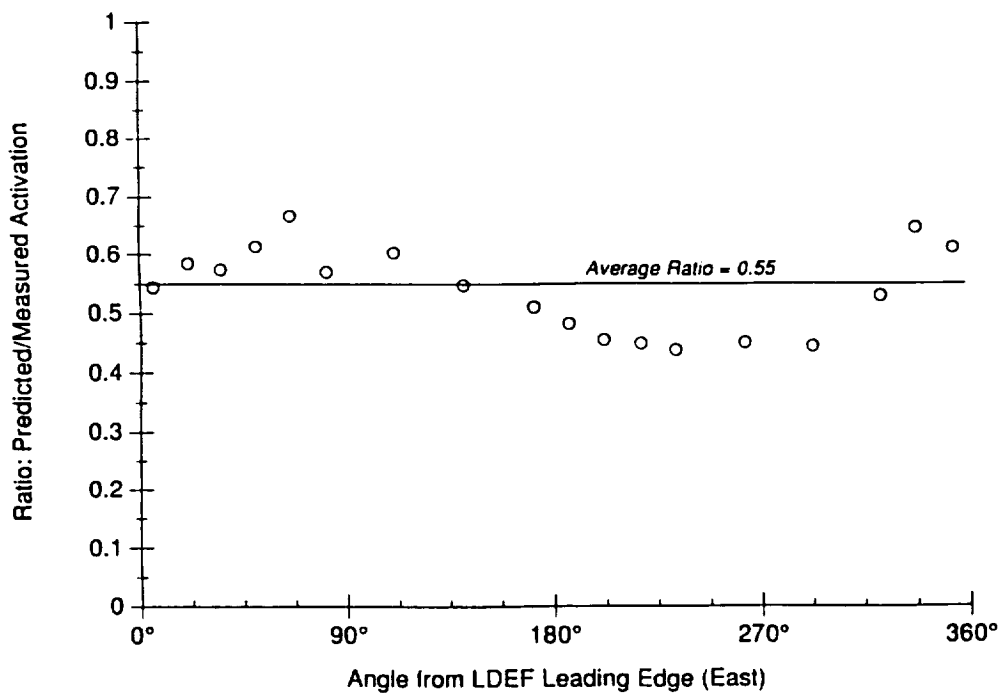
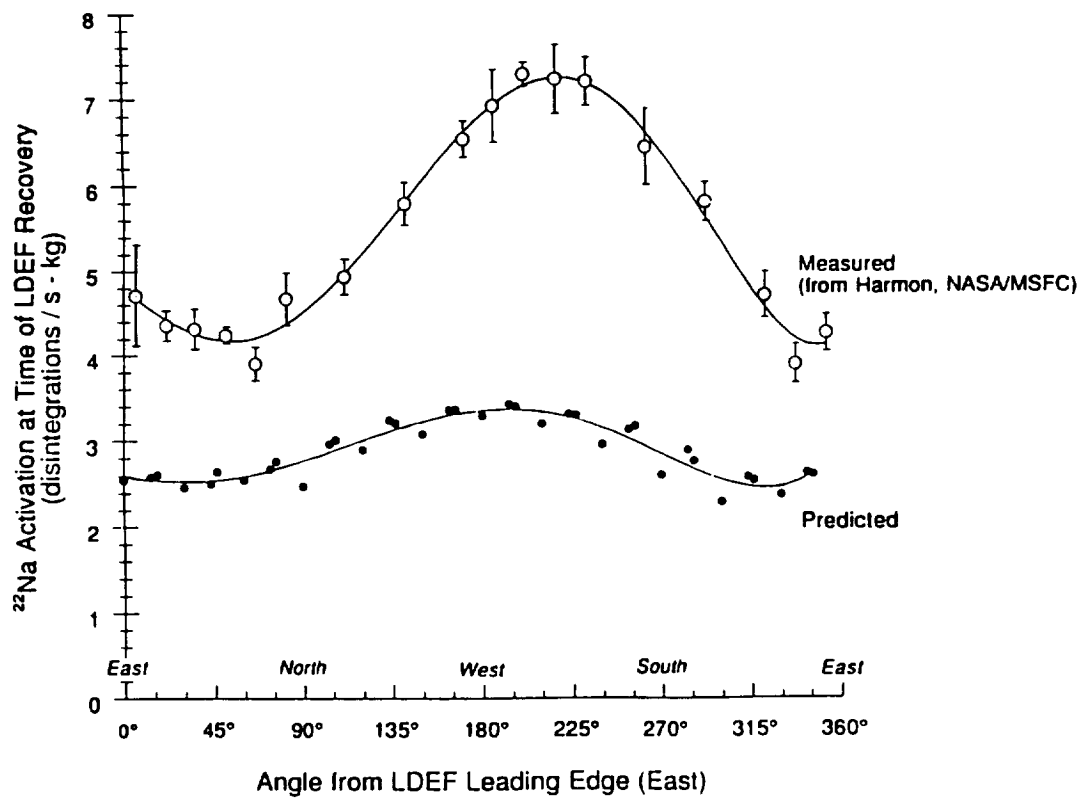


Fig. 7. Measured and predicted ^{22}Na activation of LDEF aluminum tray clamps (top), and predicted/measured ratio (bottom).

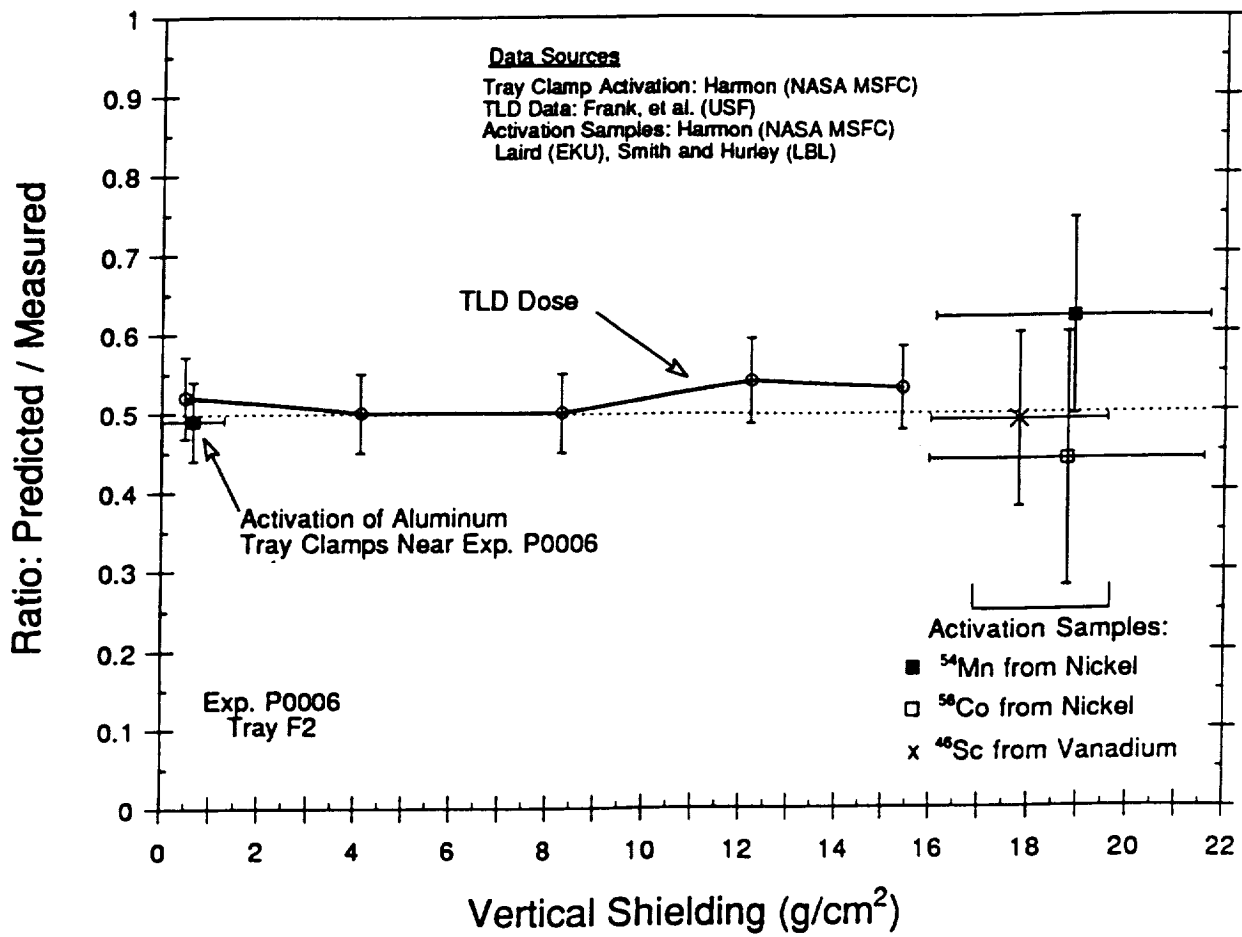


Fig. 8. Comparison of predicted vs. measured effects from trapped protons in LDEF experiment P0006 (Tray F2, trailing side).